Supporting Information

Capture and Electroreduction of CO_2 Using Highly Efficient Bimetallic Pd-Ag Aerogels Paired with Carbon Nanotubes

Maryam Abdinejad,[a] Celia Ferrag,[a,b] M. Nur Hossain,[a] Meissam Noroozifar,*[a] Kagan Kerman,*[a,b] and Heinz Bernhard Kraatz*[a,b]

Email: bernie.kraatz@utoronto.ca; kagan.kerman@utoronto.ca; m.noroozifar@utoronto.ca

a. Department of Physical and Environmental Sciences, University of Toronto Scarborough, 1265 Military Trail, Toronto, ON M1C 1A4, Canada
b. Department of Chemistry, University of Toronto, 80 At. George xStreet, Toronto, ON M5S 3H6, Canada

Table of Contents:

Part S1. Reagents and Chemicals

All reagents and solvents were of commercial reagent grade and were used without further purification, except where noted. $AgNO_3$ (99%), $CuSO_4 \cdot 5H_2O$, (99.99%), H_2SO_4 (≥99.99%), K_2CO_3 (99.99%), H_2PdCl_4 (99%), glyoxylic acid monohydrate (97%), Chloroform d (>99.8%D), Nafion perfluorinated ion-exchange resin (5%), CNT (outer diameter 13–18 nm, length 3–30 μm, purity > 99% and functional content 7.0% ± 1.5%) were purchased from Sigma-Aldrich Company. All the experimental solutions were prepared using deionized water purified by a Millipore Milli-Q water purification system (18.2 MΩ cm).

Part S2. Material Characterizations

NMR data was processed in MestreNova and chemical shifts (δ) were reported in ppm. All of the spectroscopy data for the structural characterizations were obtained using the research facilities at the University of Toronto. The gaseous products from carbon dioxide (CO_2) electro-reduction (CO, H_2) were analysed in 1 mL volumes using a gas chromatograph (PerkinElmer Clarus 680) coupled with a thermal conductivity detector (TCD) and a flame ionization detector (FID), while the liquid product was analysed using a high-resolution ABI/Sciex Qstar gas chromatography-mass spectrometer (GC-MS). The GC was equipped with a packed Molecular Sieve 5A capillary column and a packed HaySep D column. Helium (99.999%) was used as the carrier gas. A helium ionization detector (HID) was used to quantify H_2 and CO concentrations. Surface characterizations were performed using a Hitachi H7500 Scanning Electron Microscopy (SEM, Hitachi, Chiyoda, Tokyo, Japan) and a Quanta Feg 250 Field-Emission Scanning Electron Microscope.

X-ray photoelectric spectroscopy (XPS) analyses were performed with a Theta-probe Thermo-Fisher Scientific Instrument (East Grinstead, UK) with a monochromatic Kα source with a photo energy of 1486.6 eV. The accumulated angle was 90° with a 20 eV pass energy at the analyser in an 8-10 mbar vacuum chamber. The analysis area was 500 μm^2. The spectra were processed using the system's software (Avantage v5.986). A modified Shirley background was used for the baseline. A 30% Lorentzian/Gaussian mix was used for symmetric peaks; however, this was allowed to vary for the asymmetric peaks (C 1s sp^2 peak, and the main Pd 3d spin-orbit pairs). The $3d_{3/2}$ features were constrained to the $3d_{5/2}$ features for both Ag and Pd using the appropriate spin-

orbit parameters. This was also done for the Pd 3p spin-orbit pair as the O 1s peak overlaps with Pd $3p_{3/2}$ peak. Thus, by collecting the Pd $3p_{1/2}$ and applying the spin-orbit parameters, the Pd $3p_{3/2}$contribution to the O 1s peak intensity could be subtracted out.

Part S3. Synthesis of the Pd_xAg_y Aerogels

The Pd_xAg_y hydrogels, were prepared using a simple procedure. First, an aqueous solution of potassium carbonate (K_2CO_3) and glyoxylic acid monohydrate (with the ratio of 1:5) was added into a 10 mL solution of H_2PdCl_4 (0.2 mM) and $AgNO_3$ (0.2 mM) under mild stirring.[1] The mixture was then sonicated for 10 minutes to achieve a bright yellow solution.[2] Next, the glassy vial containing the suspension was transferred into the oven and allowed to settle at 70 °C for 45 min to obtain a dark grey color signifying completion of the reduction reaction. Afterwards, the temperature was decreased to 40 ℃ for another 3 h to form a black Pd_xAg_y hydrogel at the bottom of the vial. The ratio of the Pd_xAg_y hydrogels was controlled by tuning the ratio of H_2PdCl_4 and $AgNO_3$.

After the hydrogels were synthesized, they were repeatedly washed with distilled water, ethanol, and acetone (20 mL, 3 times each in sequences) followed by overnight freeze-drying using a lyophilizer to obtain porous $Pd_{0.5}Ag_{0.5}$, $Pd_{0.57}Ag_{0.43}$, $Pd_{0.67}Ag_{0.33}$, and $Pd_{0.8}Ag_{0.2}$ aerogels. The Pd_xAg_y/CNT aerogels were synthesised using a similar method by adding and dispersing 1 mg CNT in aqueous metal salt solutions. To prepare the electrode, a portion of the ground aerogels was mixed with Nafion (2%), then 2 µL of the mixture was drop casted onto a pre-cleaned GCE (0.072 cm^2) and allowed to air dry.

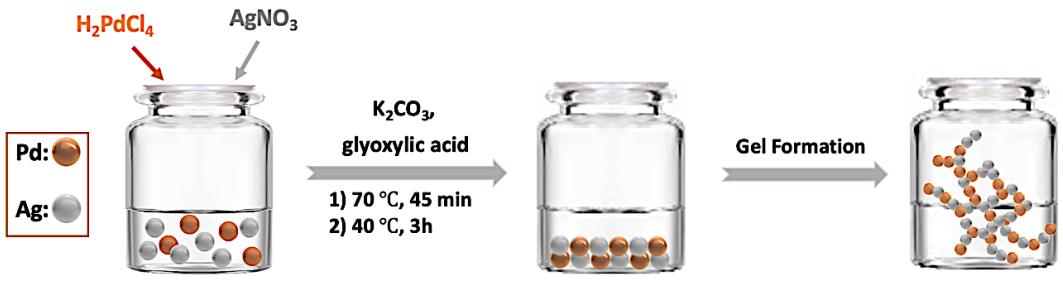

Figure S1. Schematic of the general fabrication process of Pd_xAg_y aerogels

Part S4. Electrochemical Measurements

For each electrochemical reaction, the solution was saturated with either CO_2 or Ar and the rest of the experiment was performed under sealed conditions. All of the electrolysis was performed with stirring. The electrochemical studies were carried out using a CHI 660C potentiostat (CH Instruments, Austin, TX) with a three-electrode set up enclosed in Faraday cage including: 1) aerogel-modified glassy carbon (3 mm diameter) working electrode; 2) Pt wire auxiliary electrode; 3) Ag/AgCl reference electrode. The glassy carbon surface was polished with 1, 0.3, and 0.05 μm alumina slurries. The electrodes were then ultrasonicated in acetonitrile, ethanol and water. The anode and cathode chambers were connected *via* a Nafion membrane. Cyclic Voltammetry (CV) measurements were conducted with a positive initial scan polarity, 5 second quiet, and a scan rate of 0.1 V/s. All potentials were converted from Ag/AgCl (3 M KCl) to RHE ($E_{RHE}=E^0_{Ag/AgCl}$ + 0.0591 × pH + 0.210).

The reported Faradaic efficiency (FE) and current density (*j*) are average values based on five reactions run with GC measurements taken every 15 min for 2.5 h. It should be noted that all the reported current density has been calculated based on the geometrical electrode dimensions (3mm diameter).

The FE of the CO and H_2 products was *via* either Eq. S1:

Eq. S1:

$$FE = \frac{2 \times 96485\ (\text{c/mol}) \times V\ (\text{mL/min}) \times 10^{-6}\ (\text{m}^3/\text{mL}) \times v\ (\text{vol.\%}) \times 10^5\ (\text{N/m}^2)}{8.314\ (\text{N.m/mol.K}) \times 298.15K \times I_{total}\ (\text{C/s}) \times 60\ (\text{s/min})}$$

v (vol.%) = Volume concentration of the products

V (mL/min) = Gas flow rate measured by a flow meter at room temperature under ambient pressure. I_{total} (C/s) = cell current.

Liquid products were analyzed by ^{1}H NMR spectrometry. After 2.5 h of electrolysis, 350 μL of the catholyte was mixed with 30 μL of D_2O serving as an internal standard.

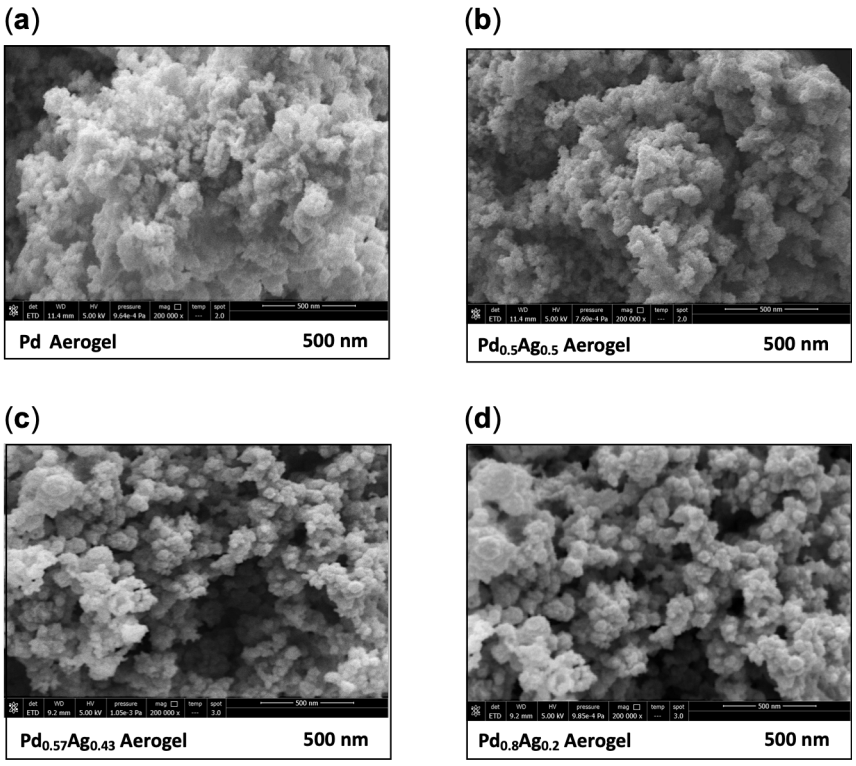

Figure S2. Scanning Electron Microscopy (SEM) of (a) Pd; (b) $Pd_{0.5}Ag_{0.5}$; (c) $Pd_{0.57}Ag_{0.43}$; and (d) $Pd_{0.8}Ag_{0.2}$ aerogels with a scale bar of 500 nm.

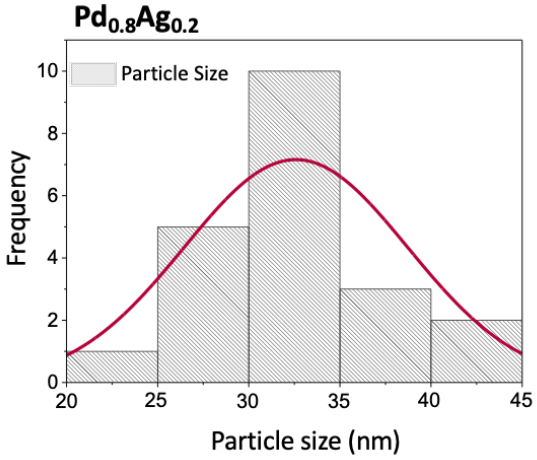

Figure S3. Particle size distribution histogram of $Pd_{0.8}Ag_{0.2}$

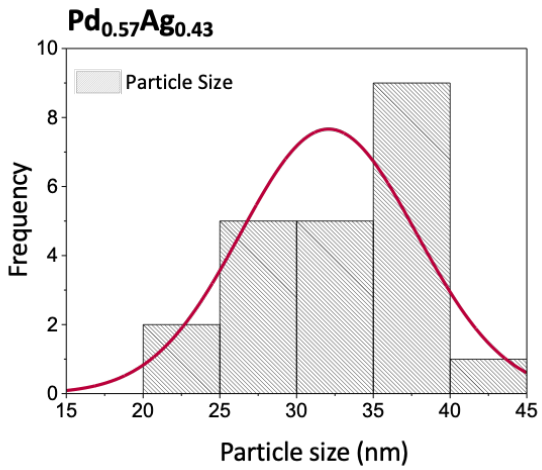

Figure S4. Particle size distribution histogram of $Pd_{0.57}Ag_{0.43}$

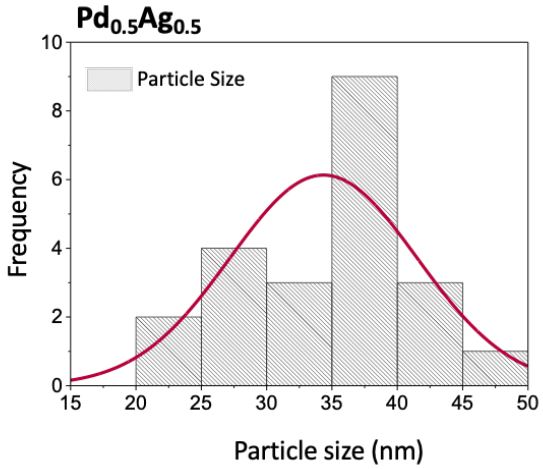

Figure S5. Particle size distribution histogram of $Pd_{0.5}Ag_{0.5}$

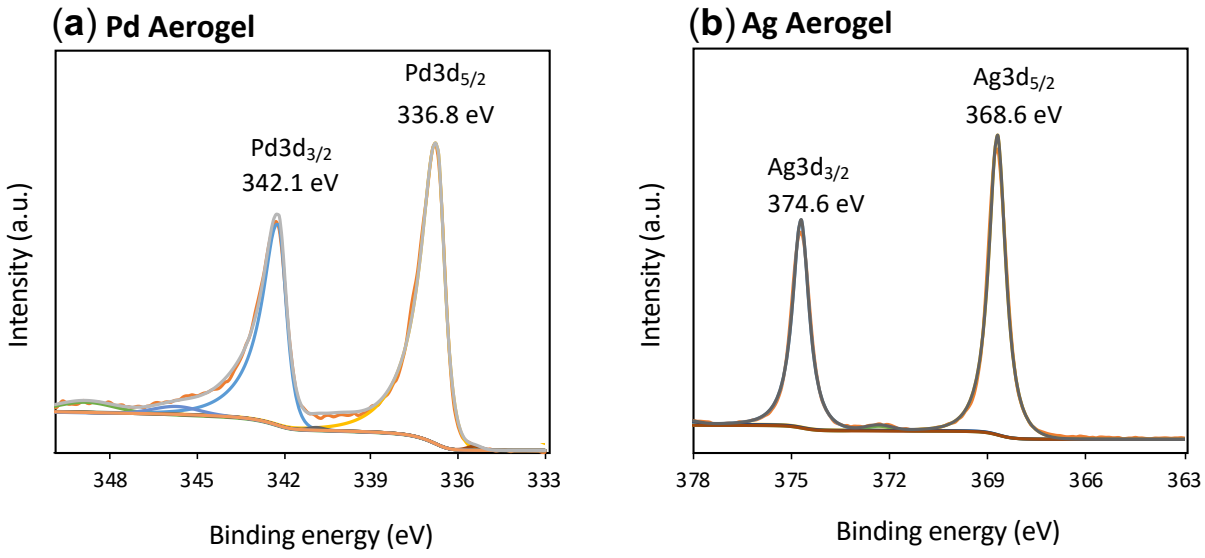

Figure S6. X-ray Photoelectron Spectroscopy (XPS) characterization of (a) Pd 3d; (b) Ag 3d of monometallic Pd and Ag aerogels.

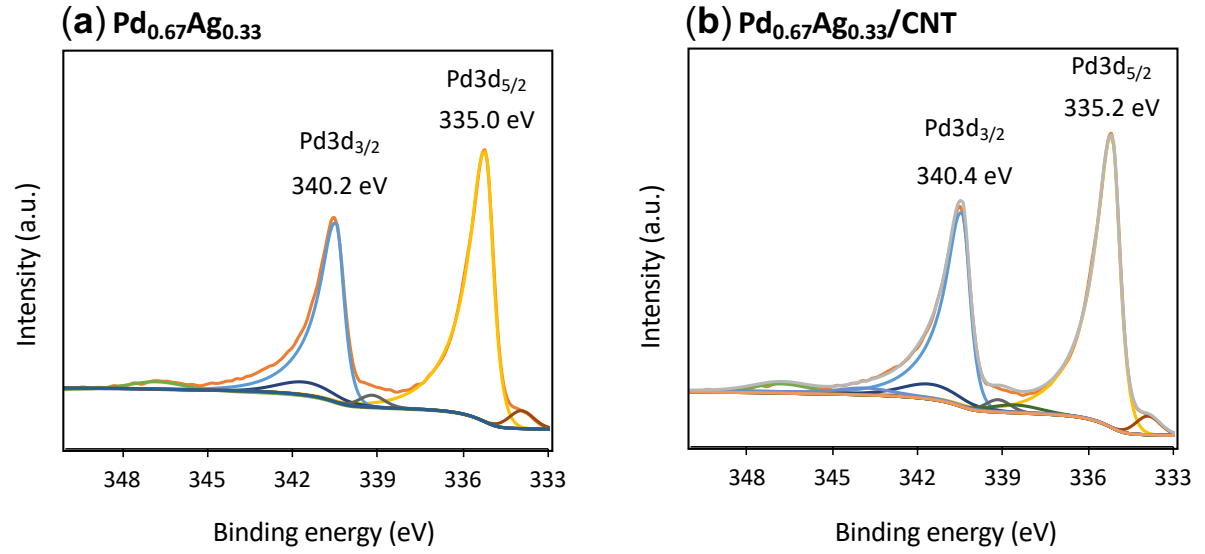

Figure S7. Pd 3d X-ray Photoelectron Spectroscopy (XPS) characterization of the bimetallic $Pd_{0.67}Ag_{0.33}$ and $Pd_{0.67}Ag_{0.33}$/CNT.

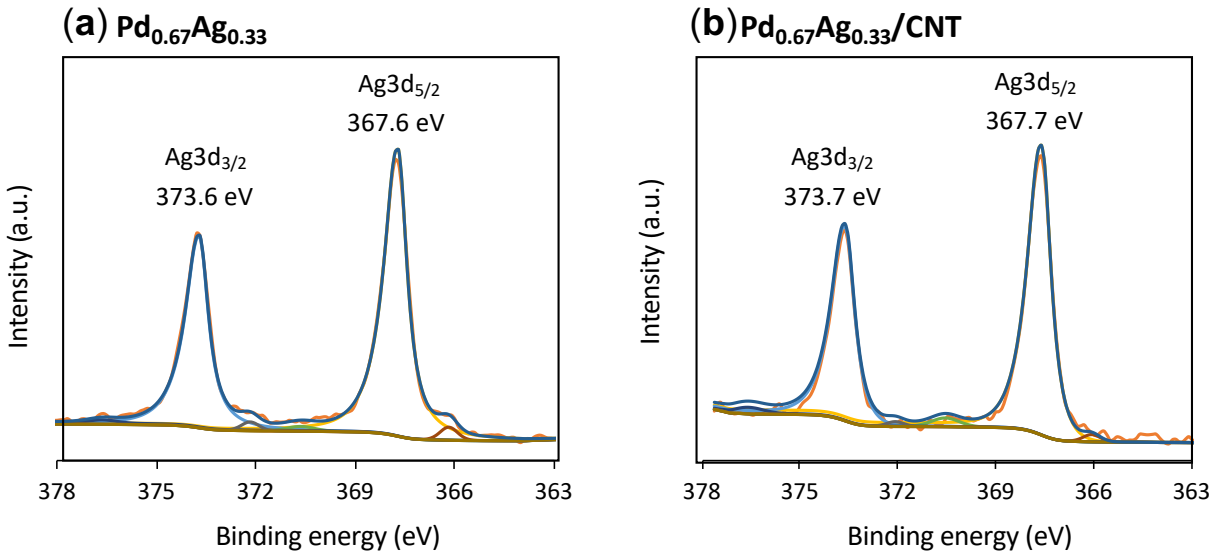

Figure S8. Ag 3d X-ray Photoelectron Spectroscopy (XPS) characterization of the bimetallic $Pd_{0.67}Ag_{0.33}$ and $Pd_{0.67}Ag_{0.33}$/CNT.

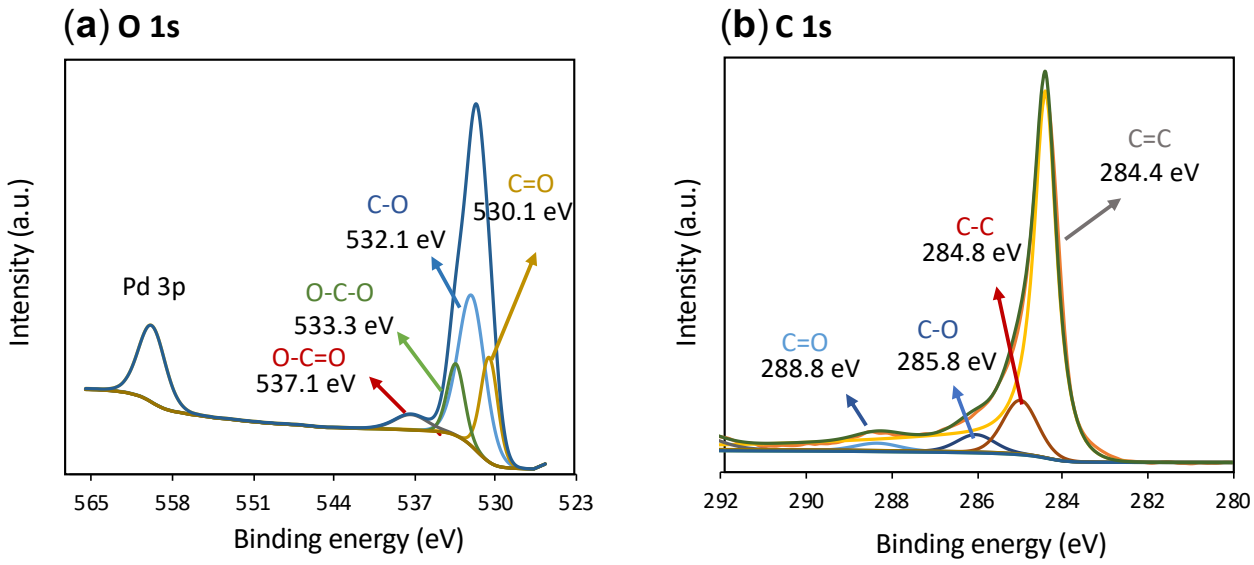

Figure S9. X-ray Photoelectron Spectroscopy (XPS) characterization of the monometallic Pd aerogel including (a) O 1s; and (b) C 1s spectra.

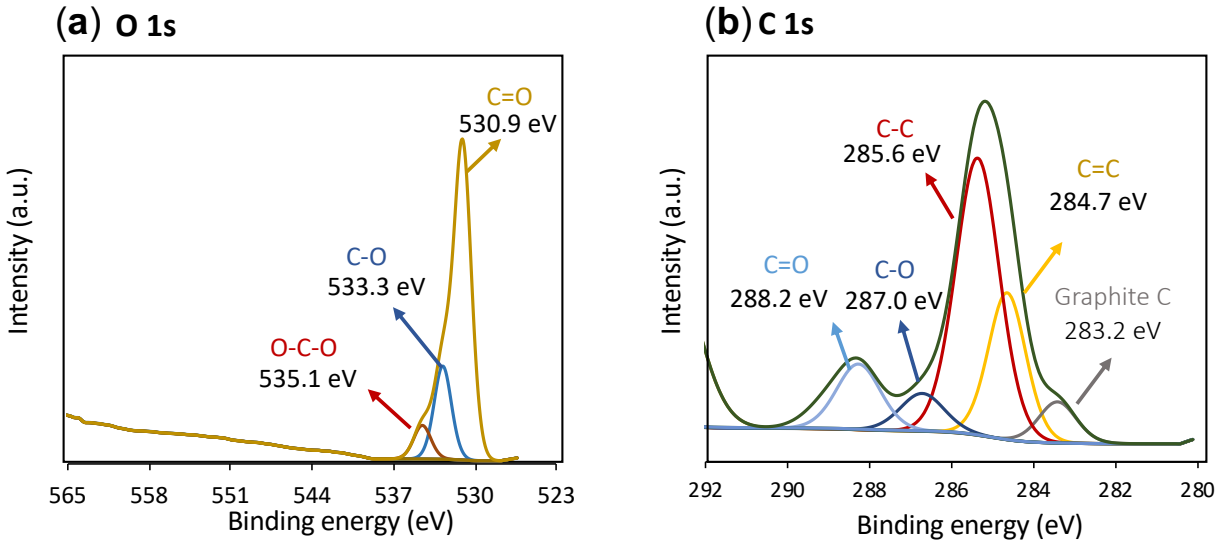

Figure S10. X-ray Photoelectron Spectroscopy (XPS) characterization of the monometallic Ag aerogel including (a) O 1s; and (b) C 1s spectra.

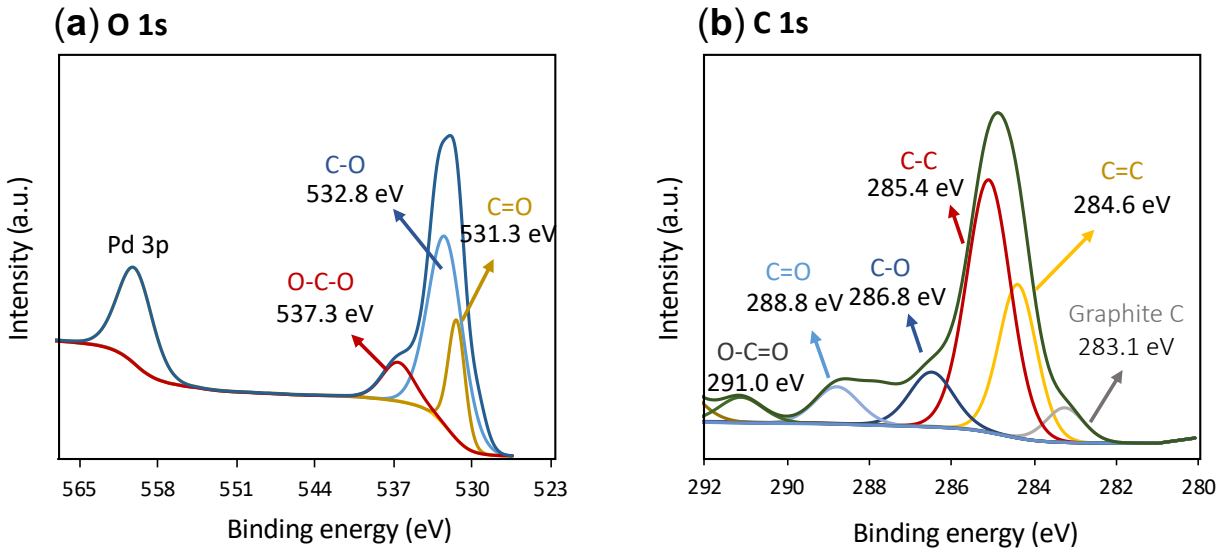

Figure S11. X-ray Photoelectron Spectroscopy (XPS) characterization of the bimetallic $Pd_{0.67}Ag_{0.33}$ aerogel including (a) O 1s; and (b) C 1s spectra.

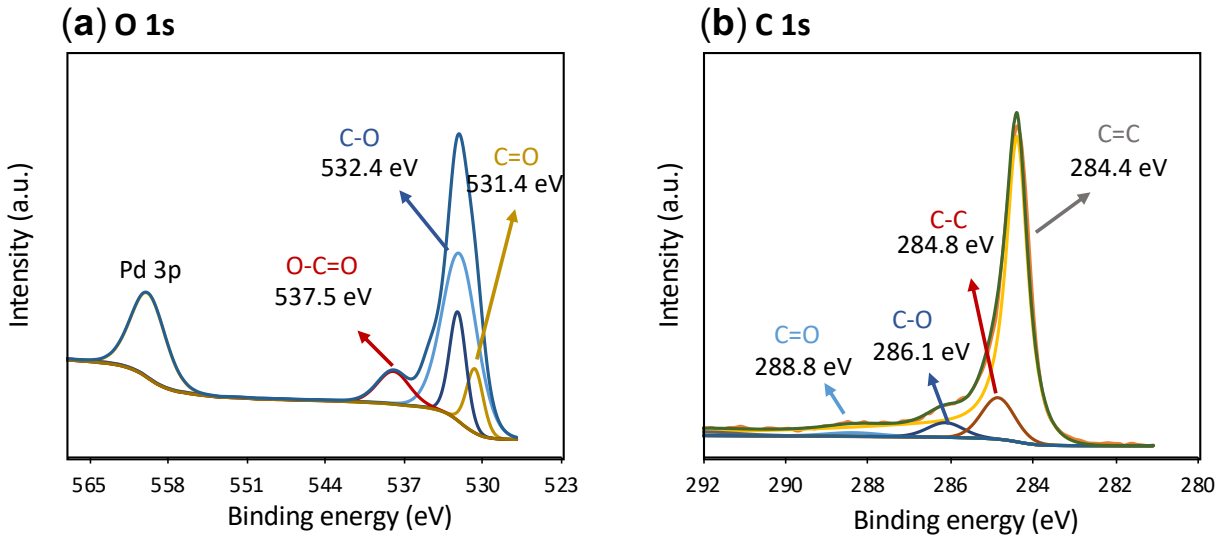

Figure S12. X-ray Photoelectron Spectroscopy (XPS) characterization of the bimetallic $Pd_{0.67}Ag_{0.33}$/CNT aerogel including (a) O 1s; and (b) C 1s spectra.

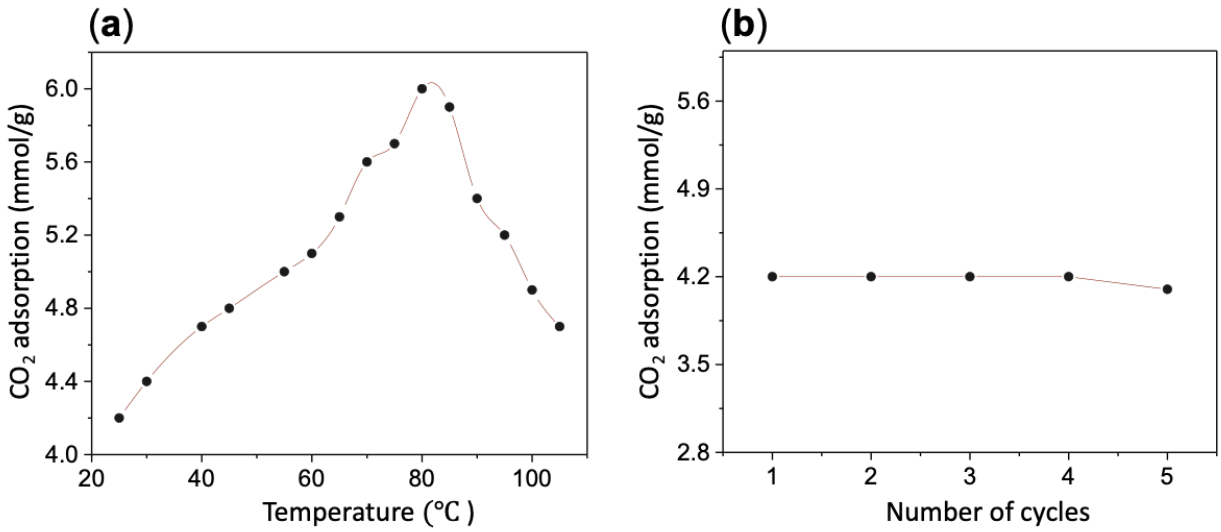

Figure S13. (a) CO_2 adsorption of $Pd_{0.67}Ag_{0.33}$ at variable temperature (25 ℃-110 ℃). (b) Cyclical adsorption/desorption of CO_2 at 80 °C, CO_2 flow rate = 50 sccm.

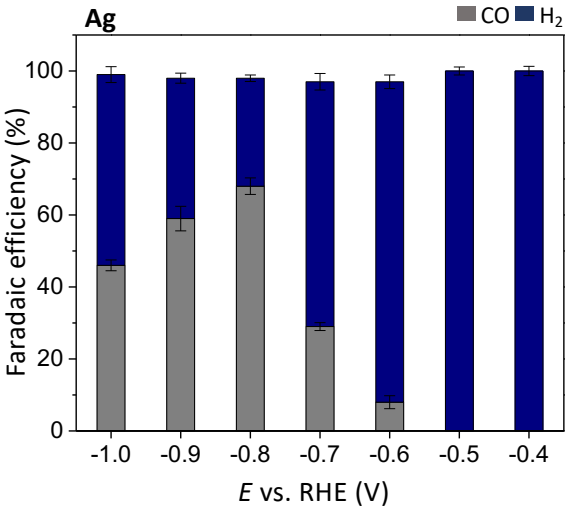

Figure S14. Faradaic efficiency (FE) of Ag aerogel after 2.5 h electrolysis at -0.4, -0.5, -0.6, -0.7, -0.8, -0.9, and -1.0 V vs. RHE in 0.1 M $NaHCO_3$.

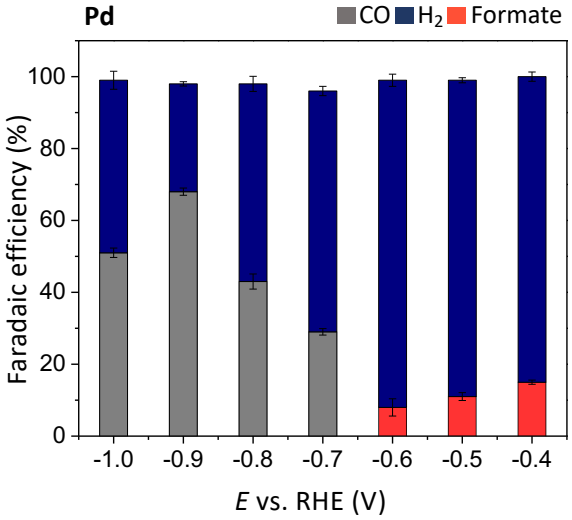

Figure S15. Faradaic efficiency (FE) of the Pd aerogel after 2.5 h electrolysis at -0.4, -0.5, -0.6, -0.7, -0.8, -0.9, and -1.0 V vs. RHE in 0.1 M $NaHCO_3$.

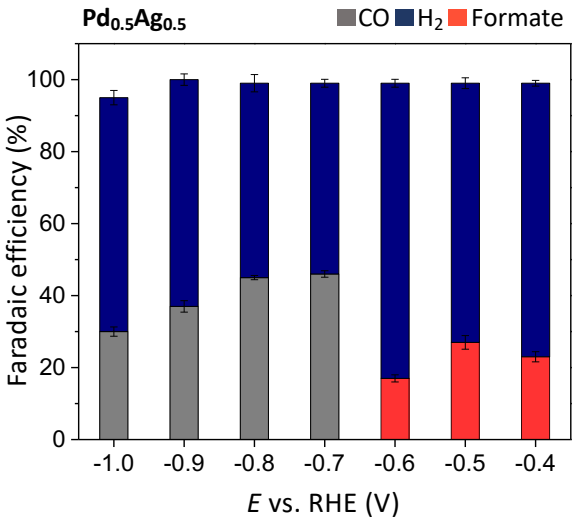

Figure S16. Faradaic efficiency (FE) of the $Pd_{0.5}Ag_{0.5}$ aerogel after 2.5 h electrolysis at -0.4, -0.5, -0.6, -0.7, -0.8, -0.9, and -1.0 V vs. RHE in 0.1 M $NaHCO_3$.

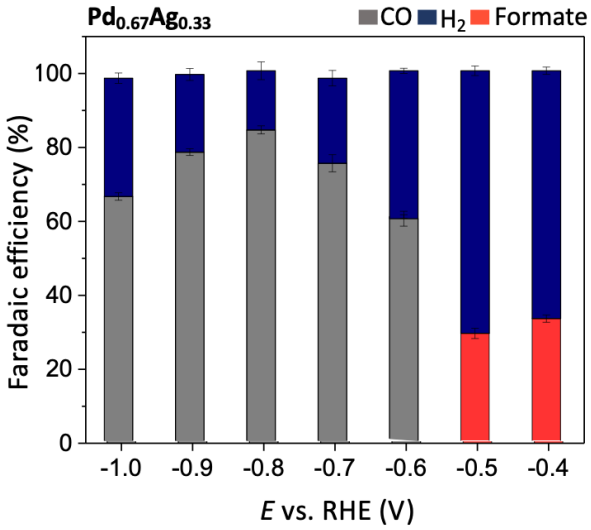

Figure S17. Faradaic efficiency (FE) of the $Pd_{0.67}Ag_{0.33}$ aerogel after 2.5 h electrolysis at -0.4, -0.5, -0.6, -0.7, -0.8, -0.9, and -1.0 V vs. RHE in 0.1 M $NaHCO_3$.

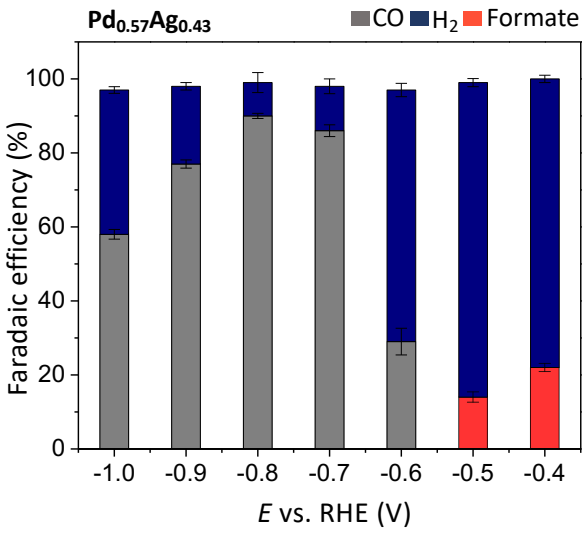

Figure S18. Faradaic efficiency (FE) of the $Pd_{0.57}Ag_{0.43}$ aerogel after 2.5 h electrolysis at -0.4, -0.5, -0.6, -0.7, -0.8, -0.9, and -1.0 V vs. RHE in 0.1 M $NaHCO_3$.

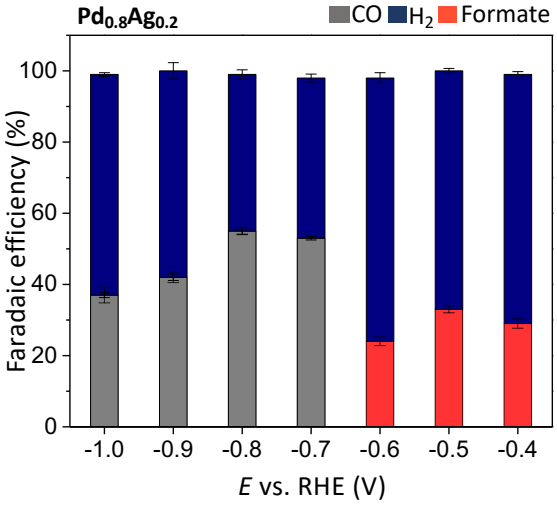

Figure S19. Faradaic efficiency (FE) of the $Pd_{0.8}Ag_{0.2}$ aerogel after 2.5 h electrolysis at -0.4, -0.5, -0.6, -0.7, -0.8, -0.9, and -1.0 V vs. RHE in 0.1 M $NaHCO_3$.

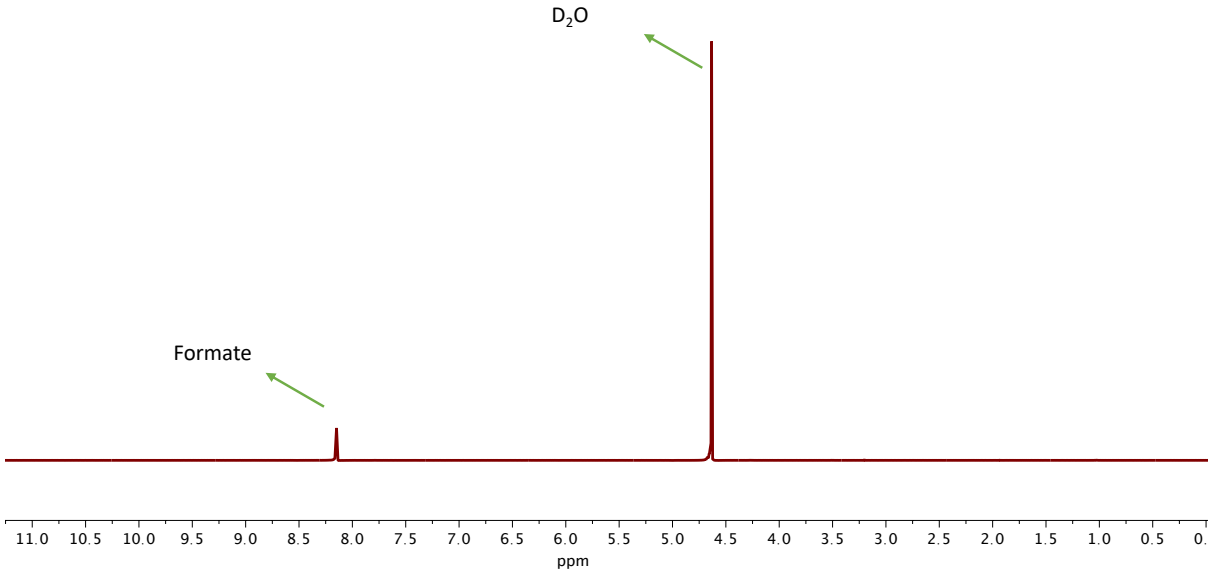

Figure S20. ^{1}H NMR spectra example of $Pd_{0.67}Ag_{0.33}$/CNT after 2 h electrolysis.

Table S1. Product analysis of the synthesized aerogels after electrochemical CO_2 reduction. The reported data are the average values of three separate measurements taken from five individual reaction runs at various potentials.

Catalyst	Electrolyte	V vs. RHE	*j* (mA/cm^2)	FE% (CO)	FE% (Formate)	FE% (H_2)	Ref.
Ag	$NaHCO_3$ (0.1 M)	-0.4	-0.33	-	-	100±1.3	Current work
	$NaHCO_3$ (0.1 M)	-0.5	-0.65	-	-	100±1.1	Current work
	$NaHCO_3$ (0.1 M)	-0.6	-1.3	8±1.8	-	89±1.9	Current work
	$NaHCO_3$ (0.1 M)	-0.7	-2.2	29±1.1	-	68±2.3	Current work
	$NaHCO_3$ (0.1 M)	-0.8	-2.6	68±2.3	-	30±0.9	Current work
	$NaHCO_3$ (0.1 M)	-0.9	-3.7	59±3.4	-	39±1.4	Current work
	$NaHCO_3$ (0.1 M)	-1.0	-4.2	46±1.5	-	53±2.2	Current work

Catalyst	Electrolyte	V vs. RHE	*j* (mA/cm^2)	FE% (CO)	FE% (Formate)	FE% (H_2)	**Ref.**
Pd	$NaHCO_3$ (0.1 M)	-0.4	-1.1	-	15±0.6	85±1.3	Current work
	$NaHCO_3$ (0.1 M)	-0.5	-1.5	-	11±1.1	88±0.7	Current work
	$NaHCO_3$ (0.1 M)	-0.6	-2.2	-	8±2.4	91±1.7	Current work
	$NaHCO_3$ (0.1 M)	-0.7	-3.8	29±0.9	-	57±1.3	Current work
	$NaHCO_3$ (0.1 M)	-0.8	-3.4	43±2.1	-	55±2.1	Current work
	$NaHCO_3$ (0.1 M)	-0.9	-6.1	68±1	-	30±0.6	Current work
	$NaHCO_3$ (0.1 M)	-1.0	-6.8	51±1.3	-	48±2.5	Current work
$Pd_{0.5}Ag_{0.5}$	$NaHCO_3$ (0.1 M)	-0.4	-2.2	-	23±1.4	76±0.8	Current work
	$NaHCO_3$ (0.1 M)	-0.5	-3.2	-	27±1.9	72±1.5	Current work
	$NaHCO_3$ (0.1 M)	-0.6	-3.4	-	17±1	82±1.1	Current work
	$NaHCO_3$ (0.1 M)	-0.7	-3.5	46±0.9		53±1.1	Current work
	$NaHCO_3$ (0.1 M)	-0.8	-3.7	45±0.6	-	54±2.4	Current work
	$NaHCO_3$ (0.1 M)	-0.9	-4.5	37±1.6	-	63±1.6	Current work
	$NaHCO_3$ (0.1 M)	-1.0	-5.1	30±1.3	-	65±2	Current work
$Pd_{0.67}Ag_{0.33}$	$NaHCO_3$ (0.1 M)	-0.4	-2.9	-	23±1	76±1	Current work
	$NaHCO_3$ (0.1 M)	-0.5	-6.8	-	11±1.4	88±1.3	Current work
	$NaHCO_3$ (0.1 M)	-0.6	-14.1	36±0.5	-	62±0.7	Current work

	Electrolyte	V vs. RHE	j (mA/cm^2)	FE% (CO)	FE% (Formate)	FE% (H_2)	**Ref.**
$Pd_{0.67}Ag_{0.33}$	$NaHCO_3$ (0.1 M)	-0.7	-20.2	75±2.3	-	23±2.1	Current work
	$NaHCO_3$ (0.1 M)	-0.8	-23.4	84±1.1	-	16±2.4	Current work
	$NaHCO_3$ (0.1 M)	-0.9	-34.0	70±0.9	-	29±1.6	Current work
	$NaHCO_3$ (0.1 M)	-1.0	-41.4	56±1	-	42±1.4	Current work
$Pd_{0.8}Ag_{0.2}$	$NaHCO_3$ (0.1 M)	-0.4	-2.4	-	29±1.1	70±0.8	Current work
	$NaHCO_3$ (0.1 M)	-0.5	-3.6	-	33±1.7	67±0.7	Current work
	$NaHCO_3$ (0.1 M)	-0.6	-5.9	-	24±3.1	72±1.5	Current work
	$NaHCO_3$ (0.1 M)	-0.7	-7.6	53±0.5	-	45±1.1	Current work
	$NaHCO_3$ (0.1 M)	-0.8	-8.2	55±1	-	44±1.3	Current work
	$NaHCO_3$ (0.1 M)	-0.9	-8.7	42±0.9	-	58±2.3	Current work
	$NaHCO_3$ (0.1 M)	-1.0	-10.2	37±0.7	-	62±0.5	Current work
$Pd_{0.57}Ag_{0.43}$	$NaHCO_3$ (0.1 M)	-0.4	-2.7	-	22±1.1	78±1	Current work
	$NaHCO_3$ (0.1 M)	-0.5	-4.6	-	14±1.1	85±1.1	Current work
	$NaHCO_3$ (0.1 M)	-0.6	-12.8	29±3.6	-	68±1.8	Current work
	$NaHCO_3$ (0.1 M)	-0.7	-16.6	62±1.6	-	36±2	Current work
	$NaHCO_3$ (0.1 M)	-0.8	-19.7	79±0.7	-	18±2.7	Current work
	$NaHCO_3$ (0.1 M)	-0.9	-24.8	57±1.1	-	43±1	Current work
	$NaHCO_3$ (0.1 M)	-1.0	-35.8	50±1.3	-	49±0.9	Current work

Catalyst	Electrolyte	V vs. RHE	*j* (mA/cm^2)	FE% (CO)	FE% (Formate)	FE% (H_2)	**Ref.**
$Pd_{0.67}Ag_{0.33}$ /CNT	$NaHCO_3$ (0.1 M)	-0.4	-4.1	-	28±2.2	70±0.8	Current work
	$NaHCO_3$ (0.1 M)	-0.5	-6.5	-	12±1	88±3.4	Current work
	$NaHCO_3$ (0.1 M)	-0.6	-27.9	45±1	-	53±1.2	Current work
	$NaHCO_3$ (0.1 M)	-0.7	-38.4	91±1.4	-	7±1	Current work
	$NaHCO_3$ (0.1 M)	-0.8	-45.8	88±2.3	-	11±1.1	Current work
	$NaHCO_3$ (0.1 M)	-0.9	-57.1	73±0.7	-	27±0.9	Current work
	$NaHCO_3$ (0.1 M)	-1.0	-60.3	59±1.1	-	38±1.4	Current work
AgNPs	EMIN-BF_4	N/A	-0.61	96	-	4	[3]
AgNPs	$KHCO_3$ (0.1 M)	- 0.7	-0.4	45	-	18	[4]
Ag foil	$KHCO_3$ (0.1 M)	-0.8	-0.01	2.2	-	75	[4]
Ag Nano-coarals	$KHCO_3$ (0.1 M)	- 0.7	-6.6	95	-	4	[4]
Nanoporous Ag	$KHCO_3$ (0.5 M)	-0.8	-0.19	92	-	7	[5]
Pd-foile	$KHCO_3$ (0.1 M)	-0.8	-1.4	28.3	-	-	[6]
PdNPs	$KHCO_3$ (1 M)	-0.7	-22.9	93.4	-		[7]
PdNPs	$KHCO_3$ (0.1 M)	-0.89	-8.9	91.2	-	-	[8]

Catalyst	Electrolyte	V vs. RHE	j (mA/cm^2)	FE% (CO)	FE% (Formate)	FE% (H_2)	Ref.
Pd/C	$KHCO_3$ (0.5 M)	-0.6	-0.3	40	-	-	9
Pd/C	$KHCO_3$ (0.5 M)	-0.1	-2.5	-	90	-	10
Pd-PAN/CNT	$KHCO_3$ (0.1 M)	-0.15	-4	-	83	-	11

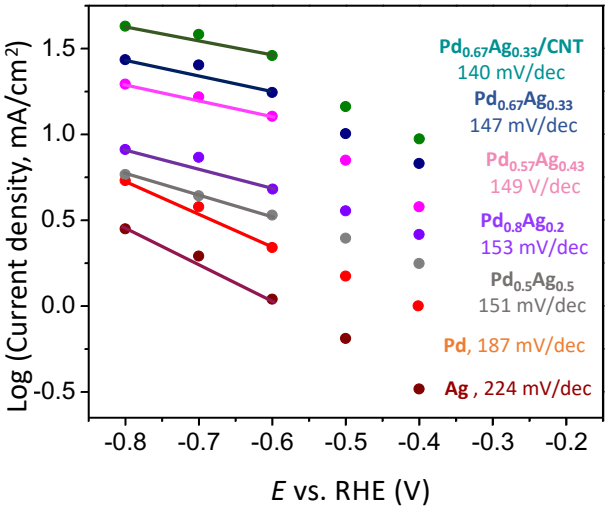

Figure S21. Tafel plots for the geometric partial current density of the CO products belongs to $Pd_{0.5}Ag_{0.5}$, $Pd_{0.57}Ag_{0.43}$, $Pd_{0.67}Ag_{0.33}$, and $Pd_{0.8}Ag_{0.2}$, and $Pd_{0.67}Ag_{0.33}$/CNT in 0.1 M $NaHCO_3$ at -0.6, -0.7, -0.8, -0.9 V vs. RHE. The Tafel slopes are indicated on the right.

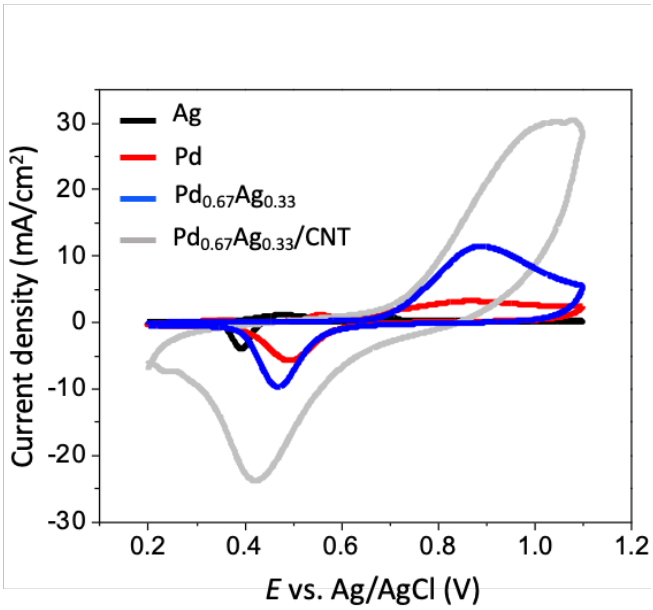

Figure S22: CVs at the scan rate of 20 mV/s of the prepared aerogel electrodes in 0.5 M H_2SO_4 + 1 mM $CuSO_4$ solution.

Table S2: Real surface area (RSA) determined by Cu under potential deposition (Cu UPD): geometric surface area of the electrode is 0.072 cm^2.

Electrode	Charge (μC)	RSA (cm^2)	Surface area increased (times)
Ag aerogel	177.35	0.44	6.2
Pd aerogel	828.57	2.04	29.1
$Pd_{0.67}Ag_{0.33}$ aerogel	1117.14	2.74	39.2
$Pd_{0.67}Ag_{0.33}$/CNT aerogel	3764.29	9.25	132.1

Part S5. References

1 A. Shafaei Douk, H. Saravani and M. Noroozifar, *Electrochim. Acta*, 2018, **275**, 182–191.

2 A. S. Douk, H. Saravani, M. Z. Yazdan Abad and M. Noroozifar, *Compos. Part B Eng.*, 2019, **172**, 309–315.

3 B. a Rosen, A. Salehi-khojin, M. R. Thorson, W. Zhu, D. T. Whipple, P. J. a Kenis and R. I. Masel, *Science.*, 2011, **334**, 643–644.

4 Y.-C. Hsieh, S. D. Senanayake, Y. Zhang, W. Xu and D. E. Polyansky, *ACS Catal.*, 2015, **5**, 5349–5356.

5 Q. Lu, J. Rosen, Y. Zhou, G. S. Hutchings, Y. C. Kimmel, J. G. Chen and F. Jiao, *Nat. Commun.*, 2014, **5**, 3242.

6 Y. Hori, H. Wakebe, T. Tsukamoto and O. Koga, *Electrochim. Acta*, 1994, **39**, 1833–1839.

7 D. Gao, H. Zhou, F. Cai, D. Wang, Y. Hu, B. Jiang, W.-B. Cai, X. Chen, R. Si, F. Yang, S. Miao, J. Wang, G. Wang and X. Bao, *Nano Res.*, 2017, **10**, 2181–2191.

8 D. Gao, H. Zhou, J. Wang, S. Miao, F. Yang, G. Wang, J. Wang and X. Bao, *J. Am. Chem. Soc.*, 2015, **137**, 4288–4291.

9 W. Sheng, S. Kattel, S. Yao, B. Yan, Z. Liang, C. J. Hawxhurst, Q. Wu and J. G. Chen, *Energy Environ. Sci.*, 2017, **10**, 1180–1185.

10 X. Min and M. W. Kanan, *J. Am. Chem. Soc.*, 2015, **137**, 4701–4708.

11 C. Zhao, Z. Yin and J. Wang, *ChemElectroChem*, 2015, **2**, 1974–1982.